Proceedings of the 3rd World Congress on Mechanical, Chemical, and Material Engineering (MCM'17)
Rome, Italy – June 8 – 10, 2017
Paper No. HTFF 148
ISSN: 2369-8136
DOI: 10.11159/htff17.148

False Transient Evaporator Thermal Model of the 'Closed Loop Two-Phase Wicked Thermosyphon (CLTPWT)' Studying Slug-Plug Liquid Vapor Flow

Karthik S. Remella, Frank M. Gerner
University of Cincinnati, Microscale Heat Transfer Laboratory
565 Rhodes Hall, Cincinnati, OH 45220, USA
sivarara@mail.uc.edu; frank.gerner@uc.edu

Abstract **–** A novel Closed Loop Two-Phase Wicked Thermosyphon (CLTPWT) was developed, fabricated, and tested by BritePointe Inc., a California based start-up, for providing thermal solutions to high power overhead light emitting diodes (LEDs). This device has structural similarities with loop heat pipes (LHPs), but the driving potential is due to a positive gravitational head (similar to a closed loop thermosyphon). The primary objective of this paper is to present a false-transient thermal model of the evaporator package of this device. The evaporator package houses of two wick structures – a sintered porous wick and a single metallic wire mesh screen (folded to form mini-channels). The sintered porous wick is centrally above the mesh screen channels. The phase change takes place inside these mini-channels and the model assumes a slug-plug two-phase flow leaving the evaporator such that the quality of the two-phase mixture is ~ 0.2. This flow regime is modeled using a time averaged uniform heat transfer coefficient obtained from nucleate flow boiling literature. The substrate temperature predictions are found to be in agreement with experimental tests conducted on the CLTPWT. It is observed that the presence of a central sintered porous wick controls the location of phase change in the mesh screen channels ensuring reliable operation of the device.

Keywords**:** Closed Loop Two-Phase Wicked Thermosyphon (CLTPWT), slug-plug flow, mesh screen channels, nucleate flow boiling

1. Introduction

Two-phase thermal management devices, such as loop heat pipes (LHPs) and close loop two-phase thermosyphons (CLTPTs), have found a wide range of applications in dissipating thermal power from microelectronic packages [1]–[5]. These devices transport thermal energy from the package to ambient air with very little thermal resistance between them. Conventional LHPs rely on pressure difference across the liquid-vapor interface (in capillary wick microstructures) for a favorable driving potential; whereas conventional CLTPTs rely on favorable hydrostatic heads for the circulation of working fluid. Apart from other operational differences, it is the presence or absence of a capillary wick structure that differentiates a conventional CLTPT from a conventional LHP. The primary reason for employing LHPs and CLTPTs, as opposed to heat pipes and two-phase thermosyphons, is because of their separated liquid-vapor flows [5]–[8]. There exists a liquid-vapor countercurrent flow in conventional heat pipes and two-phase thermosyphons which leads to flow limitations such as flooding and entrainment [9], [10]. One such two-phase heat transfer device, which bears structural resemblances to a conventional LHP but operates similar to a conventional CLTPT, was developed by BritePointe Inc., a California based start-up, for providing thermal management solutions to high power overhead light emitting diodes (LEDs) employed in high bay facilities and on factory floors [11]–[13]. Despite the presence of a wick structure in this novel device, it is currently being referred to as a *Closed Loop Two-Phase Wicked Thermosyphon (CLTPWT)*. The paper will briefly introduce this device and present a thermal model to obtain substrate temperature predictions.

The device comprises of a central evaporator package with a finned circular coil as shown in Fig. 1-(a). The evaporator and coil are connected by the liquid and vapor transport lines. The circular coil has equidistant circular fins all along its circumference. These fins enhance heat transfer by increasing the surface area. Water is employed as working fluid in this device. The quality of the two-phase mixture leaving the evaporator package is ~ 0.2 (during the steady state operation of the device). This two-phase mixture starts to condense in the finned portion of the circular coil. After

complete condensation of the working fluid, the saturated liquid starts sub-cooling in the rest of coil. Remella et al. demonstrated that the heat transfer between this finned area and ambient air is due to natural convection on the air side and obtained an empirical correlation for the same [11]. It must be highlighted here that the liquid and vapor transport lines are tilted such that the horizontal plane containing the evaporator package is lower than the circular coil. This tilt in the liquid return line ensures a positive hydrostatic head on the liquid entering the evaporator package. During the steady state operation of this device, Remella et al. [13] observed that the positive hydrostatic head due to the tilt in the transport lines is equal to the viscous/frictional pressure drop encountered by the working fluid in the sintered porous wick of the evaporator. It was also reported that the frictional pressure drop in the rest of the components were very small and therefore negligible. This allowed Remella et al. [13] to estimate the mass flow rate ($\dot{m}$) directly from the hydrostatic head (H) and permeability (κ) of the porous wick during the steady state operation of the device. It was demonstrated, both from model and experiments, that this flow rate was independent of the total input thermal power (Q_{therm}) to the CLTPWT.

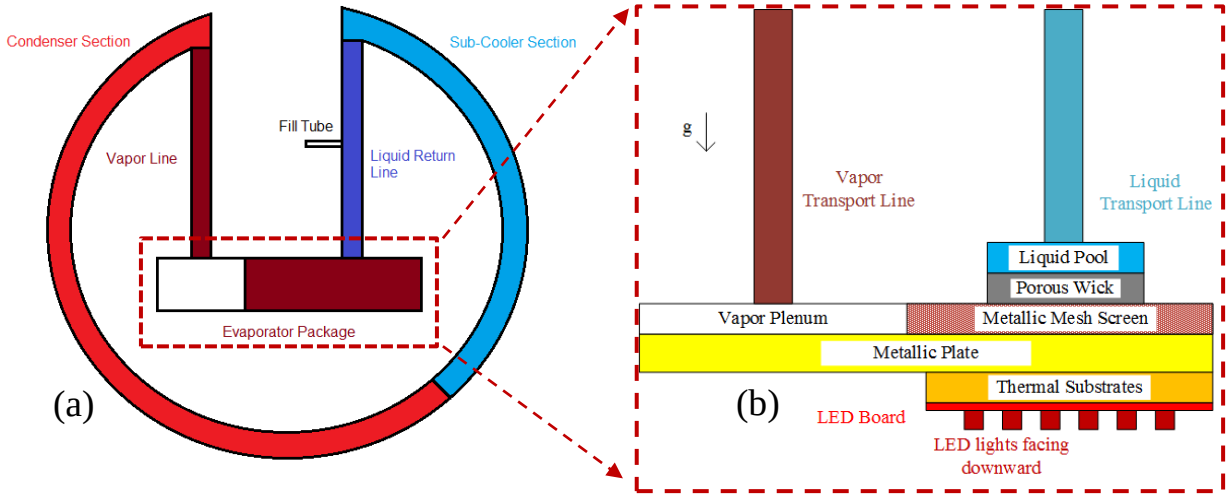

Fig. 1: (a) A simple schematic highlighting the various components of the CLTPWT, and (b) A 2D schematic of the evaporator package highlighting the various components inside.

The evaporator package, as shown in Fig. 1, comprises of a layer of thermal substrates (Fig. 2 – (a) & (c) show the 3D computer aided design (CAD) of the evaporator package). Above these thermal substrates is a conductive metallic plate. The liquid entering the evaporator package via the liquid return line has a small volume called liquid pool. Below this liquid pool, the incoming liquid encounters a sintered porous wick whose particle diameter is O(10 μm). A single layer of metallic wire mesh screen is sandwiched between the porous wick and the metallic plate. This mesh screen is folded in an accordion shape to form mini-channels; an environmental - scanning electron microscope (E-SEM) image in depicted in Fig. 2 – (d). The cross-section of these channels are assumed to be trapezoidal (Fig. 2 – (b)). The wire diameter and spacing is O(10 μm). A spacer separates the porous wick from the metallic plate and the mesh screen channels sits it (Fig. 2 – (c)). The thermal power from the microelectronics is conducted up the thermal substrates into the metallic plate. The metal wires of the screen conduct this energy and a significant portion of the input thermal power is utilized in phase change of the working fluid within the screen. This phase change process is due to either evaporation or nucleate boiling of liquid within the mesh screen. This phase change phenomenon is accompanied by relatively strong capillary forces which allow the screen to remain saturated with liquid throughout the operation of the device. Remella et al. [14] predicted the effective thermal conductivity of three geometries that approximate the mesh screen geometry. The rest of the thermal power increases the temperature of the working fluid from a lower sub-cooled temperature (T_{sc}) to the saturation temperature (T_{sat}) of the device. As mentioned earlier, a two-phase mixture quality of ~ 0.2 leaves the evaporator package through the vapor plenum and the vapor transport line. This two-phase mixture starts to condense as it enters the coil side of the device.

During a steady state operation of the CLTPWT, the flow inside these aforementioned mesh screen channels is complex. Apart from the mass flow rate, and flow conditions (location of inlet and outlet), the flow regime in the mesh screen channels predominantly depends on the phase change phenomenon. It is currently being hypothesized that the flow

inside these channels could either be a separated two-phase flow (with vapor at the bottom and liquid at the top), or a slug-plug flow with liquid and vapor bubbles leaving the evaporator. A separated flow in the channels is justified from a thin-film evaporation dominant mechanism, while a slug-plug flow is an artifact of nucleate flow boiling dominated phase change. This paper attempts to model a nucleate flow boiling phase change mechanism, with primary focus on the temperature at the thermal substrate layer. A model for an evaporation dominant phase change mechanism is currently under development, and shall be discussed in a separate paper. These models shall be compared with flow and heat transfer experiments on these mesh screen channels with appropriate inlet and outlet conditions. These results will also be reported in a separate paper.

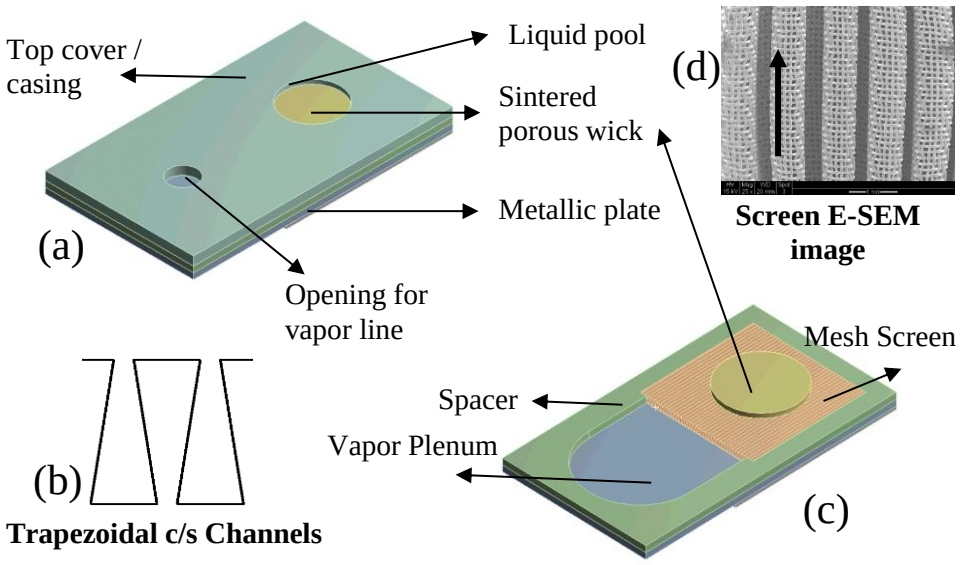

Fig. 2: (a) 3D CAD geometry of evaporator package, (b) Mesh screen c/s assumed as trapezoidal channels, (c) 3D evaporator CAD geometry without the top cover, and (d) An E-SEM image of mesh screen channels, highlighting the flow direction.

Table 1: Dimensions of various components of the evaporator.

Component	**Dimensions**
Thermal substrates	(57 x 50.8 x 1) mm^3
Metallic plate	(88.9 x 50.8 x 2) mm^3
Mesh screen	height = 2 mm, length = 40 mm, a = 820 μm, b = 250 μm
Porous wick	radius = 12.7 mm, thickness = 1.5 mm
Spacer	radius = 17.7 mm, height = 2 mm
Top cover	height = 3 mm
Vapor line	radius = 4.8 mm
Liquid pool	radius = 9.5 mm

The primary objective of this work is to predict the steady state substrate temperature for a given input thermal power (Q_{therm}). These predictions are obtained using the false-transient model discussed in this paper. A false transient approach is chosen due to lack of sufficient information regarding the steady state temperature conditions, especially on the mesh screen walls. In addition to this, the model also employed some steady state values such as saturation (T_{sat}) and sub-cooled (T_{sc}) temperature of working fluid, as obtained by Remella et al.'s coil model [13]. Assuming that the flow in the mesh screen channels is slug-plug flow, a time averaged uniform heat transfer coefficient is employed to model thermal power loss due to nucleate flow boiling. This model will also analyze the importance of the mesh screen and sintered porous wick in the evaporator.

2. Numerical Model

This section presents the numerical model and describes the necessary boundary conditions for obtaining a steady state solution of the evaporator package. In addition, it also outlines the assumptions in the model.

2.1. Assumptions

The assumptions employed in the model are delineated below.

1.The actual geometry of the mesh screen is replaced with a rectangular slab of similar thickness, whose conductivity is reported by Remella et al. [14].

2.The mesh screen is assumed to be lumped in the thickness direction i.e., the temperature of the screen across the screen thickness is uniform. This is justified by a small Biot number (a dimensionless number that relates conduction resistance to convective resistance) $\left[Bi = \frac{h_{screen}(2d_{wire})}{k_{eff}}\right]$

3.The solid particles and the adjacent liquid in the sintered porous wick are assumed to be in thermodynamic equilibrium. The justification for this assumption stems from comparing the thermal resistance of solid particles across the wick structure and that between solid and its adjacent fluid.

4.A perfect surface contact is assumed across all active components of the evaporator, i.e. the model does not account for any contact resistance between these surfaces.

2.2. False-Transient Thermal Model

The model described in this paper solves transient conduction heat equation in the evaporator. Both reheating and phase change are modeled as effective convective boundary conditions. The model also accounts for loss of thermal power due to external convection from the package via natural convection. The effective material properties employed by the model are described in the Table 2.

$$\rho C_p \frac{\partial T}{\partial t} = -\nabla.(k\nabla T) \tag{1}$$

Table 2: List of the material properties employed in the false-transient model of the evaporator.

Component	**Density, ρ** $[kg/m^3]$	**Specific heat, C_p** $[kJ/(kg.K)]$	**Conductivity, k_{eff}** $[W/(m.K)]$
Substrate, Metal plate	8933	385	400
Mesh screen	6134.2	1739.3	69.68
Spacer, Casing	7850	434	60.5
Porous wick	1825	2018.8	78.78

The following boundary conditions are employed to obtain steady state temperature predictions in this model.

1.*Uniform Heat Flux:* A uniform flux condition is employed at the bottom surface of the thermal substrate layer. During the laboratory testing of the CLTPWT, the LED board was removed and replaced with a copper heater block to measure the total input power. The application of a uniform heat flux condition replicates the testing the CLTPWT. The value of this heat flux corresponded to 171 W.

2.*Mesh Screen Walls:* As mentioned earlier in the Introduction section, the primary objective of this model is to predict the substrate temperature with a slug-plug liquid-vapor flow in the mesh screen channels of the evaporator. A time-averaged heat transfer coefficient (h_{screen}) is employed to model this phenomenon and this coefficient is obtained from literature. It was observed, from literature on flow boiling in macro/mini channels, the two-phase heat transfer coefficient varied between ~ 2,000 W/(m^2-K) to 50,000 W/(m^2-K) [15]–[18]. Most of these results were based on different working fluids such as water and R-141b, and they varied with heat flux and two-phase mixture quality. In addition to employing different mass flux, these heat transfer coefficients were estimated when the flow was unidirectional. In the current case, the flow inlet is at the center of the mesh screen channels and it exits along the channel, towards the vapor plenum. Based on this information from literature, the model attempts to conduct a parametric sweep on heat transfer coefficients ranging between 5,000 W/(m^2-K) – 25,000 W/(m^2-K). Experiments will be conducted in future to determine the exact value of this

average heat transfer coefficient. The saturation temperature of the working fluid is employed as free stream temperature in Equation (2) and its value is obtained from experiments. The detailed experimental set-up and its analysis can be found in Remella et al. [13].

$$-k_{eff}\nabla T.\vec{n} = h_{screen}(T - T_{sat}) \tag{2}$$

3. *Top Surface of Porous Wick:* The liquid requires a length scale of ~ 1.5 μm to increase its temperature from a low sub-cooled temperature (T_{sc}) to the solid wall temperature of the porous wick. This length scale was estimated using a fully developed circular pipe flow solution with constant wall temperature. Because of this conclusion, a convective boundary condition is employed on the top surface of the porous wick. This boundary condition estimates the amount of reheating undergone by the working fluid. An effective heat transfer coefficient (h_{wick}) is obtained from simple energy balance between the walls and the liquid (Equations (4) & (5)).

$$-k_{eff}\nabla T.\vec{n} = h_{wick}(T - T_{sc}) \tag{3}$$

$$h_{wick}A(T_{wick} - T_{sc}) = \dot{m}_{pore}C_p(T_{wick} - T_{sc}) \tag{4}$$

$$A = \frac{A_{pore}}{\epsilon} \tag{5}$$

Substituting Equation (5) in (4),

$$h_{wick} = \frac{\dot{m}_{total}C_p}{A_{wick}} \tag{6}$$

4. *Side Walls of Pool, Inner Walls of Plenum, & Outer Walls of Package:* Convective boundary conditions, given by Equation (7) are employed to at each of these boundary. The heat transfer coefficients employed at these boundaries all correspond to natural convection and their values, along with their respective free stream temperatures, are tabulated in Table 3.

$$-k_{eff}\nabla T.\vec{n} = h_{nat}\left(T - T_{fs}\right) \tag{7}$$

Table 3: List of h_{nat} and T_{fs} at various locations employed in the model.

Component	**Heat Transfer Coefficient, $\mathbf{h_{nat}}$ $\left[W/\left(m^2.K\right)\right]$**	**Free Stream Temp., $\mathbf{T_{fs}}$ [°C]**
Pool: Side Walls	5	T_{sc}
Package: Outer Walls	8	T_{air}
Plenum: Inner Walls	10	T_{sat}

Transient Thermal module of ANSYS, a commercial finite element solver (FEM), was employed to solve the model. A steady state solution was obtained in ~ 100 s and the solver automatically chose the appropriate solution technique for solving the model.

3. Results and Discussion

This section describes the effect of varying heat transfer coefficient on the temperatures of the porous wick, mesh screen, and thermal substrates. The obtained substrate temperature is also compared with the experimentally obtained temperature. The paper also discusses the total power lost due to nucleate flow boiling in the mesh screen, and reheating of

the working fluid in the sintered porous wick. All results reported in this paper are based on Q_{therm} = 171 W, T_{sat} = 87 ^{o}C, T_{sc} 59.2 ^{o}C, and T_{air} = 25 ^{o}C. The paper discusses the impact of 4 different h_{screen}, ranging between 5,000 W/(m^2-K) and 25,000 W/(m^2-K).

3.1. Distribution of Thermal Power

This sub-section discusses the distribution of thermal power lost in the mesh screen, and porous wick. Fig. 3 plots the various power losses through the mesh screen, porous wick, and package as a function of time. Being a false transient model, it is noted that the power loss at the porous wick and package are constant throughout the simulation. The convective power at the sintered porous wick is utilized to reheat the working fluid from a lower temperature (T_{sc}) to the temperature of the wick. A significant portion (~ 80 %, steady state) of the total thermal power (Q_{therm}) is lost through the mesh screen due to nucleate flow boiling of working fluid. A very small percentage (~ 3 %) is lost to the ambient due to natural convective heat transfer from the package. It is observed here that the convective losses from the package is approximately constant as long as $h_{package}$ represents natural convective heat transfer. In addition, the amount of power required for reheating the working fluid from T_{sc} to T_{wall} of sintered porous wick depends significantly on the effective heat transfer coefficient employed the model.

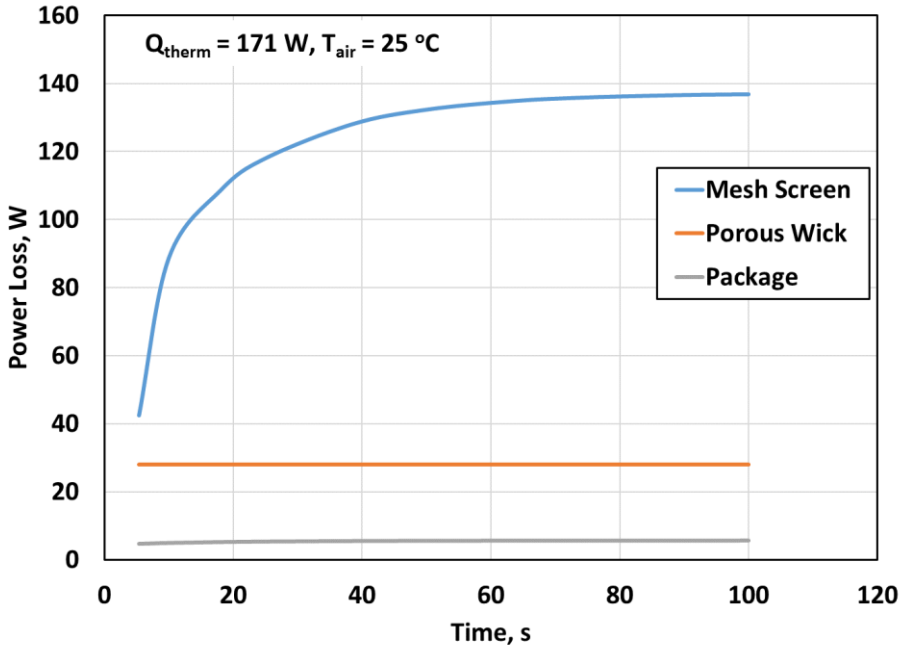

Fig. 3: Distribution of Q_{therm} to the mesh screen, porous wick, and convective loss via the package [h_{screen} = 25,000 W/(m^2-K); T_{sat} = 87 ^{o}C; T_{sc} = 59.2 ^{o}C].

3.2. Porous Wick Temperature

The sub-section reports the temperature contours on the sintered porous wick for Q_{therm} = 171 W and T_{air} = 25 ^{o}C. Fig. 4 shows contour plots of temperature of the sintered porous wick (at the wick-pool and wick-screen interfaces) for different values of h_{screen}. A significant portion of the reheating occurs at the wick-pool interface (not shown in the plot) due to the effective heat transfer coefficient. A very small percentage of reheating occurs inside the wick. The temperature at the top (wick-pool interface) is relatively cooler compared to that at the bottom (wick – screen interface). The contour plots demonstrate the solid-fluid thermodynamic equilibrium temperature in the wick. It is observed that a higher h_{screen} leads to lowering the maximum temperature of the wick. This is important for a reliable operation of the CLTPWT. A high temperature (close to T_{sat}) on the wick could lead to metastable liquid (superheated liquid) in the wick. This metastable liquid could nucleate and would lead to vapor generation in the wick. Transport of vapor from these small pores would require higher positive potential. As the device heavily relies on gravity for its driving potential, the device could stop functioning and this could eventually lead to a burn out.

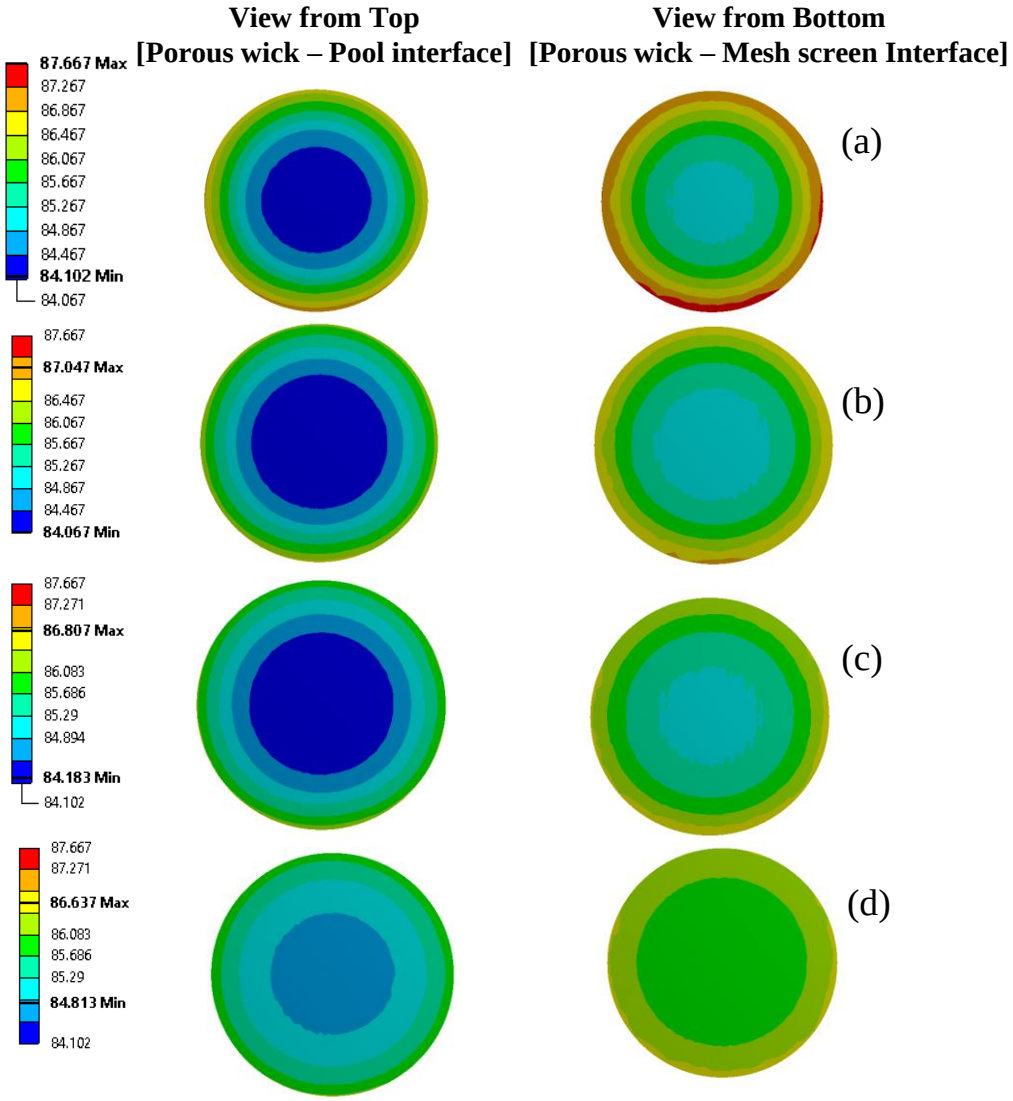

Fig. 4: Temperature contours (in ^{o}C) on sintered porous wick showing wick-pool and wick-screen interfaces for various h_{screen} [in W/(m^2-K)] of (a). 5000, (b) 7500, (c) 10,000, and (d) 25,000.

3.3. Mesh Screen Temperature

Fig. 5 shows the temperature contour plots of the metallic wire mesh screen for different h_{screen}. As observed from the plot below, it is seen that the maximum temperature of the screen decreases with increasing h_{screen}. As the total power leaving the mesh screen, due to nucleate flow boiling in the channels, is approximately constant, a higher h_{screen} leads to lower T_{screen}. As the current model does not predict the superheat required for nucleation of working fluid, it is difficult to estimate the area over which nucleation of working fluid occurs during steady state. This area, along with the flow regime of the two-phase flow, can be estimated by solving a single channel model with appropriate boundary conditions. This avenue shall be pursued in future to analyse the flow and heat transfer in a single channel.

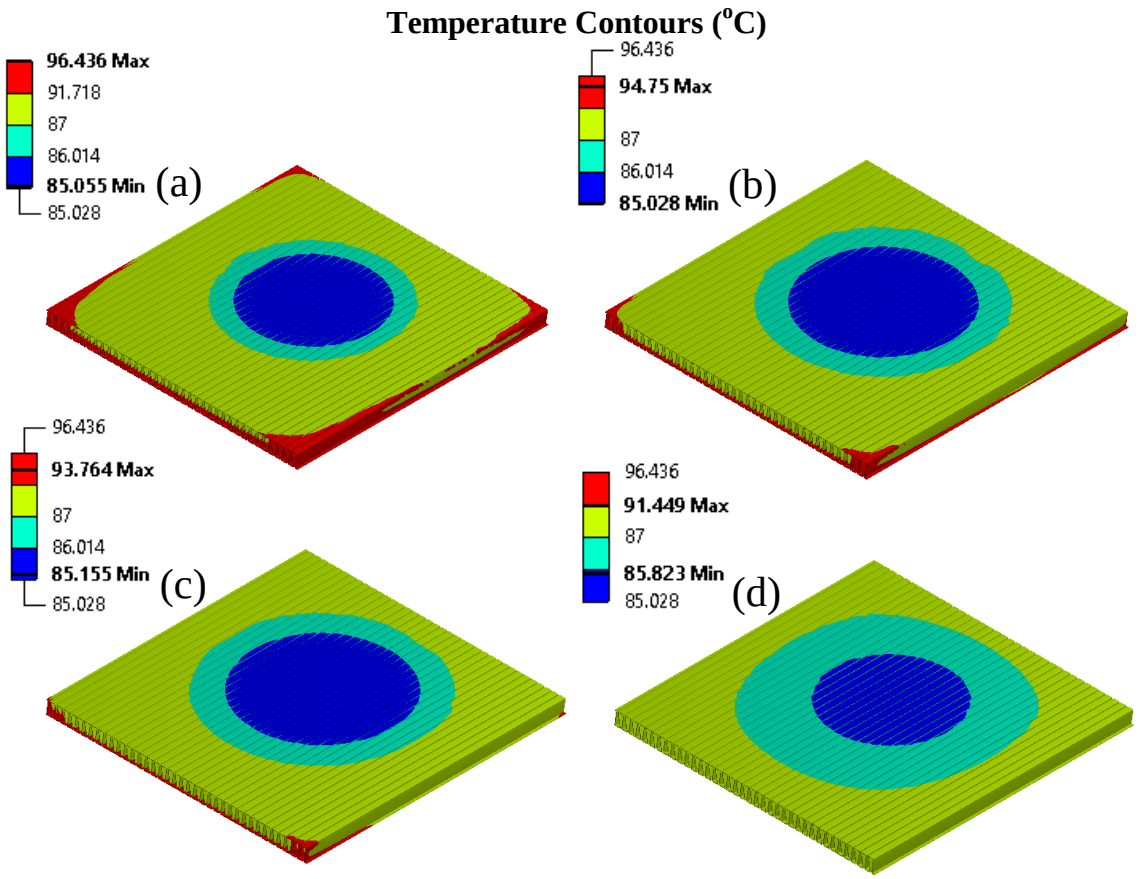

Fig. 5: Temperature contours (in ^{o}C) of metallic wire mesh screen for (a) h_{screen} = 5,000 W/(m^2-K), (b) h_{screen} = 7,500 W/(m^2-K), (c) h_{screen} = 10,000 W/(m^2-K), and (d) h_{screen} = 25,000 W/(m^2-K).

One of the striking features of Fig. 5 is the (relatively) cool central region. This is due to the presence of the central wick structure. The minimum surface area required for reheating the working fluid, from T_{wall} of the porous wick to T_{sat} + ΔT (where ΔT is representative of the superheat required for nucleate pool boiling of the working fluid), is represented by the blue and the green areas in Fig. 5. This area increases with increasing h_{screen}; although it is unclear as to what the total reheat area vs. total area over which nucleate pool boiling occurs in these channels using this model. The model is unable to predict any information on the superheat required for nucleate flow boiling.

3.4. Substrate Temperature

The substrate temperature show an increasing trend with increasing h_{screen}, as observed in Fig. 6. This is due to the fact that lower heat transfer coefficients (h_{screen}) lead to high screen temperatures, as observed in Fig. 5. Having said this, the experimentally measured temperature of 92.5 ^{o}C on the thermal substrates agrees well with all 4 heat transfer coefficients (h_{screen}) investigated in this paper. This agreement between the model and experiments, in case of h_{screen} = 5,000 W/(m^2-K), is only just. Further investigation of flow and heat transfer in the mesh screen channels is required to exactly outline the heat transfer coefficient range in them.

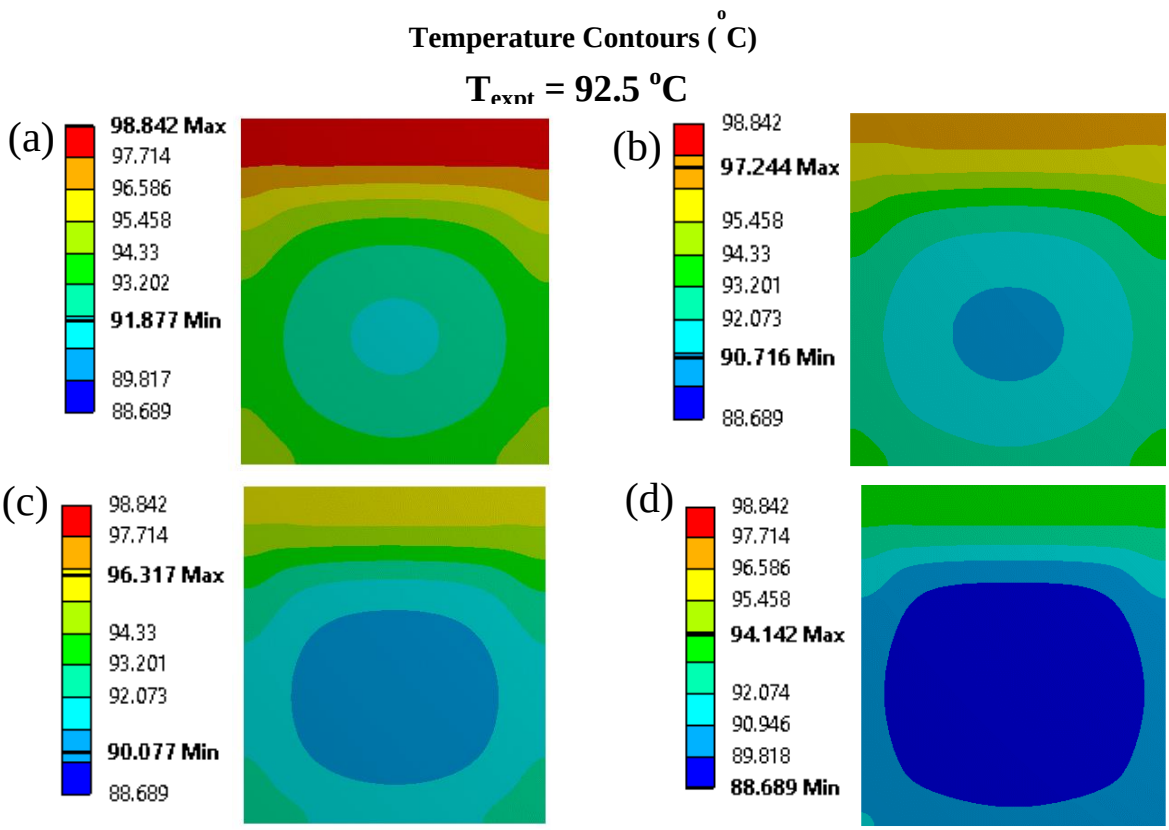

Fig. 6: Temperature contours (in ^{o}C) of thermal substrates for (a) h_{screen} = 5,000 W/(m^2-K), (b) h_{screen} = 7,500 W/(m^2-K), (c) h_{screen} = 10,000 W/(m^2-K), and (d) h_{screen} = 25,000 W/(m^2-K).

4. Concluding remarks

A false-transient heat transfer model is solved to obtain temperature contours of a particular size of the evaporator package of a novel 'Closed Loop Two-Phase Wicked Thermosyphon (CLTPWT)'. A time-averaged heat transfer coefficient is employed to model nucleate flow boiling of working fluid inside the mesh screen channels of this device. Four different heat transfer coefficients (h_{screen}), ranging between 5,000 W/(m^2-K) and 25,000 W/(m^2-K), are employed in this study. Experimentally measured substrate temperatures are found to the in good agreement with the model predictions. The main conclusions obtained from this study are as follows:

1.About 80% of total input thermal power (Q_{therm}) is utilized in phase change of the working fluid in the mesh screen channels. The total percentage of thermal power utilized in reheating the working fluid is on the order of 15%, majority of which occurs in the sintered porous wick structure.

2.The presence of porous wick structure maintains a low temperature central temperature over the mesh screen.

3.A higher heat transfer coefficient (h_{screen}) in the channel reduces the maximum screen temperature, which favourably impacts the substrate temperature.

5. Nomenclature

d	Diameter, m
h	Heat transfer coefficient, W/(m^2.K)
k	Thermal conductivity, W/(m.K)
$\dot{m}$	Mass flow rate, kg/s
A	Area, m^2
C_p	Specific heat, kJ/(kg.K)
L	Length, m

T	Temperature, ^{o}C
Sub-Scripts	
f	Fluid
fs	Free stream
sat	Saturation
sc	Sub-cooled
screen	Screen
subs	Substrate
therm	Thermal
Greek symbols	
ε	Porosity
ρ	Density

References

[1] D. Reay, R. McGlen, and P. Kew, *Heat Pipes: Theory, Design and Applications*. Butterworth-Heinemann, 2013.

[2] Y. F. Maydanik, S. V. Vershinin, M. a. Korukov, and J. M. Ochterbeck, "Miniature loop heat pipes - A promising means for cooling electronics," *IEEE Trans. Components Packag. Technol.*, vol. 28, no. 2, pp. 290-296, 2005.

[3] W. Zimbeck, G. Slavik, J. Cennamo, S. Kang, J. Yun, and E. Kroliczek, "Loop heat pipe technology for cooling computer servers," *2008 11th IEEE Intersoc. Conf. Therm. Thermomechanical Phenom. Electron. Syst. I-THERM*, pp. 19-25, 2008.

[4] Y. F. Maydanik, S. V. Vershinin, V. G. Pastukhov, and S. Fried, "Loop Heat Pipes for Cooling Systems of Servers," *IEEE Trans. Components Packag. Technol.*, vol. 33, no. 2, pp. 416-423, 2010.

[5] S. I. Haider, Y. K. Joshi, and W. Nakayama, "A Natural Circulation Model of the Closed Loop, Two-Phase Thermosyphon for Electronics Cooling," *J. Heat Transfer*, vol. 124, no. 5, p. 881, 2002.

[6] S. Launay, V. Sartre, and J. Bonjour, "Parametric analysis of loop heat pipe operation: a literature review," *Int. J. Therm. Sci.*, vol. 46, no. 7, pp. 621-636, 2007.

[7] J. Ku, "Operating Characteristics of Loop Heat Pipes," 2007.

[8] A. Franco and S. Filippeschi, "Closed loop two-phase thermosyphon of small dimensions: A review of the experimental results," *Microgravity Sci. Technol.*, vol. 24, no. 3, pp. 165-179, 2012.

[9] C. L. Tien and K. S. Chung, "Entrainment Limits in Heat Pipes," *AIAA J.*, vol. 17, no. 6, pp. 643-646, 1979.

[10] H. Nguyen-Chi and M. Groll, "Entrainment or flooding limit in a closed two-phase thermosyphon," *Journal of Heat Recovery Systems*, vol. 1, no. 4. pp. 275-286, 1981.

[11] K. S. Remella, F. M. Gerner, A. Shuja, "Steady State Parametric Modeling of Non-Convetional Loop Heat Pipes," in *Proceedings of the ASME 2013 International Mechanical Engineering Congress & Exposition*, pp. 1-12, 2013.

[12] K. S. Remella, F. M. Gerner, A. Shuja, P. Medis, "Steady State Numerical Modeling of Non-Conventional Loop Heat Pipes (LHPs)," in *ASME 2012 International Mechanical Engineering Congress and Exposition*, pp. 1467-1478, 2012.

[13] K. S. Remella and F. M. Gerner, "Simplified Mathematical Model of a novel 'Closed Loop Two-Phase Wicked Thermosyphon (CLTPWT),'" *Int. J. Therm. Sci.*, vol. 114, pp. 281-295, 2017.

[14] K. S. Remella, F. M. Gerner, "In-plane effective thermal conductivity of a single layered metallic wire-mesh screen," in *2016 32nd Thermal Measurement, Modeling & Management Symposium (SEMI-THERM)*, pp. 57-65, 2016.

[15] W. Qu, I. Mudawar, "Flow boiling heat transfer in two-phase micro-channel heat sinks-I. Experimental investigation and assessment of correlation methods," *Int. J. Heat Mass Transf.*, vol. 46, no. 15, pp. 2755-2771, 2003.

[16] S. G. Kandlikar, "Heat Transfer Mechanisms During Flow Boiling in Microchannels," *J. Heat Transfer*, vol. 126, no. 1, p. 8, 2004.

[17] S. S. Bertsch, E. a. Groll, and S. V. Garimella, "A composite heat transfer correlation for saturated flow boiling in small channels," *Int. J. Heat Mass Transf.*, vol. 52, no. 7-8, pp. 2110-2118, 2009.

[18] C. L. Ong and J. R. Thome, "Macro-to-microchannel transition in two-phase flow: Part 1 - Two-phase flow patterns and film thickness measurements," *Exp. Therm. Fluid Sci.*, vol. 35, no. 1, pp. 37-47, 2011.